Discrete Time Crystals Enforced by Floquet-Bloch Scars

Biao Huang,[1,*] Tsz-Him Leung,[2] Dan M. Stamper-Kurn,[2,3,4] and W. Vincent Liu[5,6,†]
[1]Kavli Institute for Theoretical Sciences, University of Chinese Academy of Sciences, Beijing 100190, China
[2]Department of Physics, University of California, Berkeley, California 94720, USA
[3]Challenge Institute for Quantum Computation, University of California, Berkeley, California 94720, USA
[4]Materials Sciences Division, Lawrence Berkeley National Laboratory, Berkeley, California 94720, USA
[5]Department of Physics and Astronomy and IQ Initiative, University of Pittsburgh, Pittsburgh, Pennsylvania 15260, USA
[6]Shenzhen Institute for Quantum Science and Engineering, Southern University of Science and Technology, Shenzhen 518055, China

(Received 20 May 2022; accepted 29 August 2022; published 19 September 2022)

We analytically identify a new class of quantum scars protected by spatiotemporal translation symmetries, dubbed Floquet-Bloch scars. They are distinguished from previous (quasi-)static scars by a rigid spectral pairing only possible in Floquet systems, where strong interaction and drivings equalize the quasienergy corrections to all scars and maintain their spectral spacings against generic bilinear perturbations. Scars then enforce the spatial localization and rigid discrete time crystal (DTC) oscillations as verified numerically in a trimerized kagome lattice model relevant to recent cold atom experiments. Our analytical solutions offer a potential scheme to understand the mechanisms for more generic translation-invariant DTCs.

DOI: 10.1103/PhysRevLett.129.133001

Introduction.—Systems far from equilibrium have become a fertile ground cultivating unexpected phenomena recently. Among them, discrete time crystals (DTC) [1–7] constitute an intriguing example. As foundational concepts of ground state and temperature fall apart in the absence of thermal equilibrium, Landau's theory of symmetry breaking [8] is replaced by new principles like spectral pairing and eigenstate orders [1,2] in handling time translation symmetries. That results in the DTC phenomena where Hamiltonians $\hat{H}(t+T)=\hat{H}(t)$ give rise to observables $O(t+NT)=O(t)$ $(1<N\in\mathbb{Z})$ oscillating like a temporal charge (or spin) density wave. Crucially, the periodicity NT demands no fine-tuning and withstands generic perturbations.

The concept of DTCs has been considered in several physical realizations [9–15]. While the strongly disordered cases are relatively well understood [1–3,16], the possibility of DTCs in translation-invariant ordered systems is less clear. Empirical evidence for DTCs is accumulating in both physical and numerical experiments [9,10,17–23]. However, analytical explanations based on many-body localization (MBL) [24] or prethermalization [25] do not seem to apply to these cases. Recently, it was indicated that quasiconservation laws [26,27], which can be enhanced by single-particle terms, may help protect phenomena pertinent to DTCs. Meanwhile, the initial state dependence of clean DTCs [26,28] has been reexamined in terms of scar physics [29] in recent numerics [30,31]. Altogether, continued investigation on DTCs in nondisordered systems, with the objectives of uncovering the underlying mechanism that supports the DTC and the specific role of many-body (vs. single-particle) effects, is warranted.

In this Letter, we gain insights on these two research objectives by studying a small cluster of soft-core bosons on driven trimerized kagome lattices, relevant to recent experiments [32] and feasible for numerical verifications. We find analytically that it is a class of quantum scars *protected by* spatiotemporal translation invariance, dubbed Floquet-Bloch scars (FBS), that gives rise to DTC behaviors for sublattice density oscillations. FBSs identified here *neither* exploit a static scar (i.e., PXP model [29,33,34]) *nor* end up with engineered static Hamiltonians. Instead, these FBSs exhibit a unique DTC feature. Specifically, each scar's quasienergy may be shifted considerably under perturbation. However, the interplay of strong interactions and drivings equalizes the scar level shifts, which is proved to all orders in our perturbative treatment. Then, the quasienergy difference ω_0 between FBSs remains invariant and enforces the persisting $2\pi/\omega_0$-periodic DTC. Rigid scar level spacing here resembles the "spectral pairing rigidity" for all Floquet eigenstates in MBL DTCs [1,16]. Also, such a mechanism allows for rather generic perturbations compared with preexisting scar models typically relying on microscopic details to achieve configuration separations [29,33–44]. Thus, our analytical solutions not only offer a more definitive understanding of clean DTC mechanisms, but also point out a new way of constructing scars showing peculiar spectral orders characteristic of Floquet systems.

Model and phenomena.—We consider bosons evolving under a Hamiltonian $\hat{H}(t+T)=\hat{H}(t)$ that is toggled between two settings repetitively within each period T:

$$\hat{H}_1 T/2\hbar=\phi_1\sum_{\boldsymbol{r},\mu\neq\nu} i f_{\mu\nu}[\hat{\psi}^\dagger_{\boldsymbol{r}\mu}\hat{\psi}_{\boldsymbol{r}\nu}+\lambda\hat{\psi}^\dagger_{\boldsymbol{r}+\boldsymbol{e}_\mu,\mu}\hat{\psi}_{\boldsymbol{r}+\boldsymbol{e}_\nu,\nu}],\ t\in[0,T/2)$$
$$\hat{H}_2 T/2\hbar=\sum_{\boldsymbol{r},\mu}[\phi_2\hat{n}_{\boldsymbol{r}\mu}(\hat{n}_{\boldsymbol{r}\mu}-1)+\theta_\mu\hat{n}_{\boldsymbol{r}\mu}],\ t\in[T/2,T). \quad (1)$$

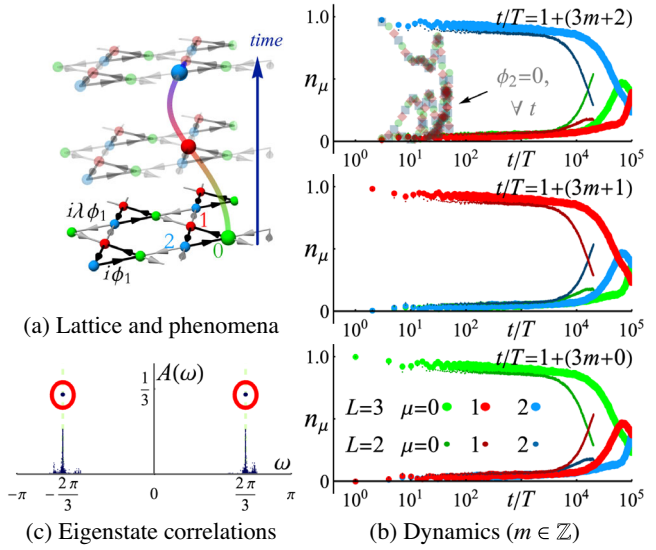

FIG. 1. (a) Trimerized kagome lattice and the schematic illustration of DTC dynamics. Triangles with strong (weak) bonds are denoted by black (gray) colors, with $+i$ hopping directions indicated by arrows. (b) Particle dynamics $n_\mu(NT) = \sum_{\boldsymbol{r}}\langle\psi_{\rm ini}|(\hat{U}_F^\dagger)^N n_{\boldsymbol{r}\mu}\hat{U}_F^N|\psi_{\rm ini}\rangle$, with the initial state $|\psi_{\rm ini}\rangle$ at $t/T = 1$ when all particles locate at a single site $\boldsymbol{r} = \boldsymbol{0}$, $\mu = 0$. To facilitate reading, data are grouped into three sets at t mod $3T = 0,\ 1,\ 2$ respectively. For comparison, the noninteracting $\phi_2 = 0$, $L = 3$ case is plotted at all t in the upper panel as translucent dots. (c) Temporal correlation functions indicating infinite-time response frequencies ($L = 3$). Unless denoted otherwise, $N_b = 5$, $\phi_1 = 2\pi/3\sqrt{3}$, $\lambda = 0.1$, $\phi_2 = 1.1$, and $\theta_{1,2,3} = (0.1, 0.2, -0.3)$.

Here, $\hat{H}_1$ describes the hopping of noninteracting bosons in a trimerized kagome lattice with complex hopping amplitudes, as shown in Fig. 1(a), while $\hat{H}_2$ describes the combination of on site single-particle and interaction energy shifts. Dimensionless parameters $(\phi_1, \lambda, \phi_2, \theta_\mu)$ characterize the Floquet operator $\hat{U}_F = P_t e^{-(i/\hbar)\int_0^T dt\hat{H}(t)} = e^{-i\hat{H}_2 T/2\hbar}e^{-i\hat{H}_1 T/2\hbar}$. $\hat{\psi}_{\boldsymbol{r}\mu}$ and $\hat{n}_{\boldsymbol{r}\mu} = \hat{\psi}^\dagger_{\boldsymbol{r}\mu}\hat{\psi}_{\boldsymbol{r}\mu}$ are annihilation and particle number operators respectively, for L^2 unit cells $\boldsymbol{r} = m_1\boldsymbol{e}_1 + m_2\boldsymbol{e}_2$ ($m_{1,2} = 0, 1, \ldots, L-1$) and three sublattices $\mu, \nu = 0, 1, 2$. Here $\boldsymbol{e}_{1,2}$ are Bravais vectors for kagome lattices, and $\boldsymbol{e}_0 \equiv \boldsymbol{0}$. $if_{\mu\nu} = (1 + 2e^{2\pi i(\mu-\nu)/3})/\sqrt{3} = \pm i$ specifies the $+i$ hopping directions in Fig. 1(a). Note that $\sum_\mu \theta_\mu = 0$ can always be achieved by subtracting $(N_b/3)\sum_\mu \theta_\mu$ from $\hat{H}_2 T/2\hbar$, where total bosons $N_b = \sum_{\boldsymbol{r}\mu}\hat{n}_{\boldsymbol{r}\mu}$.

DTC dynamics obtained by exact diagonalization is briefly shown in Fig. 1. When $\lambda \to 0$, $\hat{H}_1$ enters the strongly trimerized regime composed of disconnected triangles, where $\pi/2$ fluxes equalize the spacing between single-particle flat bands $\omega_n = 0, \pm\sqrt{3}\phi_1$ ($\hat{U}_F|\omega_n\rangle = e^{i\omega_n}|\omega_n\rangle$). Then, $\phi_1 = 2\pi/3\sqrt{3}$ leads to $3T$ ballistic oscillations for particles $\hat{U}_F^\dagger\hat{\psi}^\dagger_{\boldsymbol{r},\mu=0,1,2}\hat{U}_F = \hat{\psi}_{\boldsymbol{r},\mu=1,2,0}$ breaking the Hamiltonian time translation symmetry of T, as in Fig. 1(a). Frequencies given by single-particle physics are, of course, unstable against perturbations. It is then the hallmark for DTC where strong interactions ϕ_2 stabilize the $3T$ periodicity without fine-tuning; see Fig. 1(b). Late time dynamics can be further confirmed by the temporal correlation functions $C(\omega) = \sum_{N=-\infty}^{\infty}(e^{i\omega N}/2\pi)\times \sum_n\langle\omega_n|\hat{P}(N)\hat{P}(0)|\omega_n\rangle = \sum_{mn}\delta(\omega - \omega_{mn})A(\omega_{mn})$ for the sublattice density bias, i.e., $\hat{P}(N) = (\hat{U}_F^\dagger)^N N_b^{-1}\sum_{\boldsymbol{r}}(\hat{n}_{\boldsymbol{r}0} - \hat{n}_{\boldsymbol{r}1})\hat{U}_F^N$. Note that the summation N is over *infinite* time without truncation. The spectral weight $A(\omega_{mn}) = |\langle\omega_m|\hat{P}|\omega_n\rangle|^2$, $\omega_{mn} = \omega_m - \omega_n$ in Fig. 1(c) showing strong peaks at frequencies $\omega_0 \to \pm 2\pi/3 + O(1/D)$ verifies long-time oscillation periods $2\pi T/|\omega_0| \to 3T$. The small deviation $O(1/D)$ suppressed by Hilbert space dimension D gives an envelop modulation in Fig. 1(b) as noticed previously for both MBL [2,16] and clean [17] DTCs.

The above phenomena may be viewed from several angles. Particularly, in the case of complete trimerization, $\lambda = 0$, the two-dimensional lattice breaks up into isolated trimers. DTCs observed in this case are then explained simply as that of a microscopic three-site chiral system similar to Ref. [45]. If we were to regard intertrimer coupling as simply opening up each one-trimer DTC to an external bath composed of other trimers, we might expect the overall DTC dynamics to be destroyed over short time at $\lambda \neq 0$ [46]. Yet, such expectations contradict results in Figs. 1(b) and 1(c). Below, we offer an explanation that DTCs in the coupled-trimer regime are stabilized by a special class of scar Floquet eigenstates each spanning over the entire two-dimensional lattice.

Identifying scars.—Quantum scars are rare nonergodic eigenstates within an eigenstructure that is otherwise thermalizing [47]. Numerical calculations confirm the overall thermalizing, nonintegrable nature of our model system. Specifically, we point to two signatures of nonintegrability: level-spacing statistics and entanglement entropy.

Consider first the level spacing. Ordering quasienergies as $\omega_n < \omega_{n+1}$, following Ref. [48], we test for ergodicity by calculating the level spacing ratios $r_n = \min(\delta_n, \delta_{n+1})/\max(\delta_n, \delta_{n+1})$ for consecutive gaps $\delta_n = \omega_{n+1} - \omega_n$. Clearly from Fig. 2(a), except for a vanishingly small region in proximity to single particle limit $\phi_2 \to 0$, our model is generically far from the integrable Poissonian case $\langle r\rangle \to 0.39$. We also note a crossover between two ergodic Gaussian orthogonal (GOE) or unitary (GUE) ensembles purely by different drivings, an interesting feature previous seen in spin models [49].

We next exploit the entanglement entropy (EE) to examine each Floquet eigenstate $|\omega_n\rangle$. Reduced density matrices $\rho_A = \mathrm{Tr}_B(|\omega_n\rangle\langle\omega_n|)$ for subsystem A [region enclosed by highlighted paths in Fig. 2(b)] can be formed

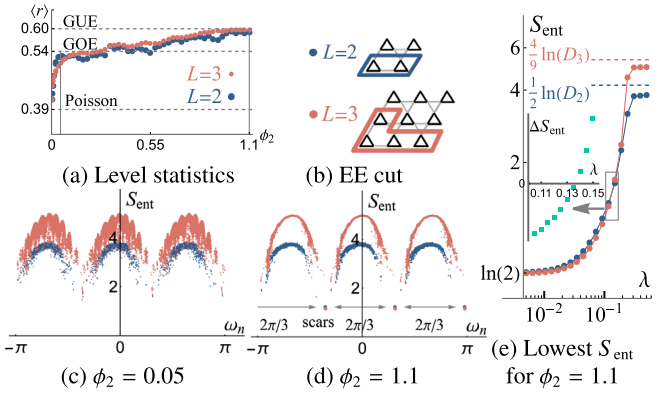

FIG. 2. (a) $\langle r\rangle$ shows generic ergodicity. (b) Subsystem for computing EE. (c) and (d) Eigenstate EE in (c) proximate-integrable and (d) DTC regimes, where low-entropy scars in (d) are highlighted by larger dots. (e) Lowest EE approaching size-insensitive values at small λ and volume law $S_{\rm ent} \sim (N_{\rm sub}/3L^2)\ln(D_L)$ at large λ. Here D_L is the total Hilbert space dimension and $N_{\rm sub}$ the subsystem site number enclosed in (b). Inset: $\Delta S_{\rm ent} = S_{\rm ent}^{(L=3)} - S_{\rm ent}^{(L=2)}$ near the crossing $\lambda_0 \approx 0.135$. Unless specified otherwise, in all plots parameters are the same as in Fig. 1. Blue (or red) colors denote $L = 2$ (or $L = 3$) respectively.

by tracing out the remaining part B in real space. The EE $S_{\rm ent} = -{\rm Tr}(\rho_A \ln \rho_A)$ then shows that in both proximate-integrable [Fig. 2(c)] and DTC [Fig. 2(d)] regimes, majority eigenstates do exhibit the typical arch shape for $S_{\rm ent}$ whose values increase with Hilbert space dimensions [50]. The narrow distribution of EE for eigenstates of similar quasienergy in the DTC regime confirms that majority arch eigenstates are ergodic [50], consistent with $\langle r\rangle$ results previously.

However, in the DTC regime, additional nonergodic states are observed. As exhibited in Fig. 2(d), we identify precisely $3L^2$ low $S_{\rm ent}$ scar states (each scar dot in the figure is L^2-fold degenerate). Each set of scars separates from the others by quasienergy $|\Delta E| \to 2\pi/3$, corresponding exactly to the DTC frequency in Fig. 1(c). The scaling of lowest EE in Fig. 2(e) shows a system size L insensitive scar EE for $\lambda \to 0$. With increasing λ, a possible transition is observed around $\lambda_0 \approx 0.135$ [51], after which all eigenstates approach the volume law ergodic limit.

We have confirmed numerically that the parameters in Fig. 2(c) give a rather short DTC lifetime, unlike the lifetime shown in Fig. 1(b) for the parameters in Fig. 2(d). It strongly indicates that the DTC behaviors here are intimately associated with scars rather than (approximate) overall integrability.

Analytical results for FBS.—To characterize these quantum scars further, we work in the many-body momentum basis [52] $|\boldsymbol{k}, \{n_{\boldsymbol{r},\mu}\}\rangle = (1/L)\sum_{m_1,m_2=0}^{L-1} e^{(2\pi i/L)(k_1 m_1 + k_2 m_2)} |\{n_{\boldsymbol{r}+m_1\boldsymbol{e}_1+m_2\boldsymbol{e}_2,\mu}\}\rangle$ constructed from Fock basis $|\{n_{r\mu}\}\rangle = \prod_{r\mu}[(\hat{\psi}^\dagger_{r\mu})^{n_{r\mu}}/\sqrt{n_{r\mu}!}]|0\rangle$. Here $\{n_{r\mu}\}$ specifies occupation numbers at different sites, and $\boldsymbol{k} \sim k_{1,2} = 0, 1, \ldots, L-1$. Then, translation-invariant $\hat{U}_F$ are block diagonalized $\langle \boldsymbol{k}, \{n_{r\mu}\}|U_F|\boldsymbol{k}', \{n'_{r\mu}\}\rangle \sim \delta_{\boldsymbol{k},\boldsymbol{k}'}$. Each $\boldsymbol{k}$ sector would be shown later to host three scar states, leading to the $3 \times L^2$-fold scars in Fig. 2(d).

It is helpful to write down the solution $U_F|\boldsymbol{k}, \ell, \{n_{r\mu}\}\rangle = e^{iE(\ell,\{n_{r\mu}\})}|\boldsymbol{k}, \ell, \{n_{\boldsymbol{r}}\}\rangle$ to Eq. (1) at the anchor point $\lambda = 0$,

$$|\boldsymbol{k}, \ell, \{n_{r\mu}\}\rangle = \frac{1}{\sqrt{3}}\sum_{m=0,1,2} e^{-i(\frac{2\pi m}{3}\ell - \alpha_m)}|\boldsymbol{k}, \{n_{\boldsymbol{r},\mu+m \bmod 3}\}\rangle, \quad (2)$$

$$E(\ell, \{n_{r\mu}\}) = \frac{2\pi}{3}\ell + \phi_2 \sum_{r\mu} n_{r\mu}(n_{r\mu} - 1), \quad \ell = 0, \pm 1, \quad (3)$$

where $\alpha_0 = 0$, $\alpha_1 = \sum_{r\mu}\theta_\mu n_{r\mu}$, and $\alpha_2 = -\sum_{r\mu}\theta_\mu n_{\boldsymbol{r},\mu+2 \bmod 3}$. Each eigenstate populates three sublattices $\mu = 0, 1, 2$ coherently, and therefore an arbitrary Fock state $|\{n_{r\mu}\}\rangle$, usually taken as initial states, will simultaneously overlap with all three branches $\ell = 0, \pm 1$ separating from each other by quasienergy $|\Delta E| = 2\pi/3$. Then, observables diagonal in the Fock basis, such as $\hat{O} = \hat{n}_{r\mu}$ or $\hat{O} = \hat{P} = N_b^{-1}\sum_{\boldsymbol{r}}(\hat{n}_{\boldsymbol{r}0} - \hat{n}_{\boldsymbol{r}1})$, will demonstrate an oscillation $\langle\hat{O}\rangle(t) \sim c_1^* c_2 \langle \boldsymbol{k}_1, \ell_1, \{n_{r\mu}\}|\hat{O}|\boldsymbol{k}_2, \ell_2, \{n_{r\mu}\}\rangle e^{-i\Delta E t/T} +$ c.c. with periodicity $2\pi T/\Delta E = 3T$.

Spectral pairing ΔE for the majority of eigenstates in Eqs. (2) and (3) is, as expected, unstable against perturbations. The crucial difference here from the disordered case [1–3,16] is the uniform interaction strength ϕ_2 in Eq. (3), which results in an enormous Floquet emergent degeneracy. Specifically, consider the combination $Q_a = \{(q_j^{(a)}, N_j^{(a)})|j = 1, 2, \ldots, M\}$ for, i.e., $q_j^{(a)}$ copies of sites each hosting $N_j^{(a)} \geq 0$ particles. In terms of the Hubbard interaction $\phi_2 \sum_{r\mu} n_{r\mu}(n_{r\mu} - 1) = \phi_2 \sum_j q_j^{(a)} N_j^{(a)}(N_j^{(a)} - 1)$, each Q_a manifold contains degenerate levels of different $\{n_{r\mu}\}$ as $\deg(Q_a) = (3L^2)!/\prod_{j=1}^M q_j^{(a)}!$. The degeneracy, though partially lifted by $2\pi\ell/3$ in Eq. (3), leads to the instability that a small perturbation could generally trigger a reconstruction for extensive numbers of eigenstates in Eq. (2) with different configurations $\{n_{r\mu}\}$, leading to the ergodicity as indicated by Fig. 2. Correspondingly, a Fock initial state would overlap with large numbers of eigenstates with different quasienergies without rigid spectral pairings.

To identify FBS, we then seek manifolds with low degeneracy. Except for a homogeneous distribution $n_{r\mu} = N_b/3L^2$ (deg = 1) without dynamical signatures, the lowest degenerate $\{n_{r\mu}\}$ deposits all N_b bosons into a single site $n_{r\mu} = \delta_{\boldsymbol{r},\boldsymbol{r}_0}\delta_{\mu,\mu_0}N_b$. There are apparently $3L^2$ such $\{n_{r\mu}\}$ with N_b bosons allocated into different sites $(\boldsymbol{r}_0, \mu_0)$. They compose the FBS eigenstates

$$|\boldsymbol{k}, \ell, N_b\rangle = \frac{1}{\sqrt{3}}\sum_{m=0,1,2} e^{-i(\frac{2\pi m}{3}\ell - \alpha_m)}|\boldsymbol{k}, \quad \{n_{r\mu} = \delta_{\boldsymbol{r},\boldsymbol{0}}\delta_{\mu,m}N_b\}\rangle, \quad (4)$$

with quasienergy $E_{\rm scar}(\ell) = 2\pi\ell/3 + \phi_2 N_b(N_b-1)$. The $3L^2$ FBSs equally partition into L^2 conserved many-body momentum $\boldsymbol{k}$ sectors, each hosting three scars with $\ell = 0, \pm 1$. Spatial translation symmetry then forbids hybridizing eigenstates of different $\boldsymbol{k}$, and temporal translation symmetry protects the conserved quasienergy separating different ℓ by $|\Delta E| = |E_{\rm scar}(\ell+1) - E_{\rm scar}(\ell)| = 2\pi/3$. Therefore, FBSs experience no degenerate-level perturbations.

It still remains to consider nondegenerate perturbations. In particular, the periodicity 2π of Floquet quasienergy constrains the Hubbard-interaction gap for different Q_a to be of the order unity. Then, one may expect each scar level to receive an energy correction $\sim\lambda^2$ (of Fermi golden rule type), resulting in fast detuning within $t \sim T/\lambda^2 \sim 100T$ for $\lambda = 0.1$. However, such estimations directly contradict Fig. 1(b).

The resolution turns out to be that all three $\ell = 0, \pm 1$ scars are shifted identically, such that their quasienergy difference, dubbed *spectral pairing* gap $|\Delta E| = 2\pi/3$ [53], is unchanged. In the Supplemental Material [54], we construct the strong-drive perturbation theory. For conciseness, we illuminate the essential physics below by elaborating results up to the second order in the perturbation series, while higher orders cases are left to the Supplemental Material [54].

Arrange a Floquet operator in the form $U_F = U_0 U'$, where U_0 corresponds to Eq. (1) at $\lambda = 0$, and perturbations are factored into $U' \equiv e^{i\lambda H'}$. For our purposes, it is more than enough to take H' as a generic hopping Hamiltonian $H' = \sum J_{r\mu\neq r'\mu'} \hat{\psi}^\dagger_{r\mu} \hat{\psi}_{r'\mu'}$. (See the Supplemental Material [54] for the factorization process). Scar quasienergy corrections $e^{i\tilde{E}_{\rm scar}(\ell)} = e^{i[E_{\rm scar}(\ell) + \sum_{\alpha=1}^{\infty} \lambda^\alpha E^{(\alpha)}_\ell]}$ up to the second order read as $E^{(1)}_\ell = \langle \boldsymbol{k}, \ell, N_b | H' | \boldsymbol{k}, \ell, N_b \rangle$, $E^{(2)}_\ell = -\frac{1}{2} \sum'_{(\ell', \{n_{r\mu}\})} |\langle \boldsymbol{k}, \ell', \{n_{r\mu}\} | H' | \boldsymbol{k}, \ell, N_b \rangle|^2 \cot\{[E_{\rm scar}(\ell) - E(\ell', \{n_{r\mu}\})]/2\}$, where summation $\sum'$ excludes the scar eigenstate in consideration. Here, $E^{(1)}_\ell = 0$ is trivially identical for all ℓ. Importantly, Eqs. (2)–(4) show that each term for $E^{(2)}_\ell$ depends only on the difference $(\ell - \ell')$. Because of 2π quasienergy periodicity, quantum numbers ℓ in Eqs. (2) and (3) are only defined modulo 3. That allows for shifting dummy indices ℓ' in the summation $E^{(2)}_{\ell_1} \equiv \sum'_{\ell', \{n_{r\mu}\}} \varepsilon(\ell_1 - \ell') = \sum'_{\ell', \{n_{r\mu}\}} \varepsilon[\ell_2 - (\ell' - \ell_1 + \ell_2)] = \sum'_{\ell'', \{n_{r\mu}\}} \varepsilon(\ell_2 - \ell'') = E^{(2)}_{\ell_2}$, proving the equality of energy corrections for all scars. The Supplemental Material [54] also numerically verifies spectral pairing rigidity for Eq. (1) and against more generic bilinear perturbations.

Importantly, it is exactly the Floquet spectrum periodicity that allows for shifting all three ℓ's in Eq. (3) by the same integer and ends up with an identical set of levels, which is crucial for the above proof. In the Supplemental Material [54], we prove that the spectral pairing rigidity persists to *all perturbation orders* for FBSs. Therefore, $O(L^2)$ initial states overlapping with multiple FBSs separating by a rigid $\omega_0 = 2\pi/3T$ will exhibit persisting $2\pi/\omega_0 = 3T$ DTC oscillations.

Analytical identification of FBSs and proof for their spectral pairing rigidity are the main results of our Letter. They rely on three pivotal factors. First, *strong interactions* validate the starting point from Eqs. (2) and (3) for kicked Fock states. Second, *strong Floquet drivings* produce three identical $\ell = 0, \pm 1$ spectral plethora at $\lambda = 0$, and the 2π quasienergy periodicity intrinsic of Floquet nature enables the rigid spectral pairing for FBS against perturbations. Third, *spatiotemporal translation symmetry* prevents FBS from mutual hybridization. Therefore, FBSs describe genuine strongly interacting Floquet matters in clean systems.

Numerical verification.—Revisiting previous numerics can now be illuminating. Spectral function peaks in Fig. 1(c) derive from pairs of FBSs in Eq. (4), $A(\omega_0)|_{\lambda\to 0} = |\langle \boldsymbol{k}, \ell_1, N_b | \hat{P} | \boldsymbol{k}, \ell_1 \pm 1, N_b \rangle|^2 = 1/3$, $|\omega_0| = 2\pi/3$. The spectral pairing rigidity then stabilizes $|\omega_0|$ against perturbation up to finite size effects, resulting in DTC oscillations in Fig. 1(b). Also, Eq. (4) prescribes an L-independent EE for FBS at $\lambda \to 0$ (see the Supplemental Material [54] for analytical calculation) as in Fig. 2(e).

Finally, we offer an efficient way to benchmark FBS by exploiting their peculiar $\boldsymbol{k}$ space localization. A natural measure is then the momentum space inverse participation ratio $\mathrm{IPR} = \sum_{\{n_r\}} |\langle \boldsymbol{k}, \{n_{r\mu}\} | \omega_n \rangle|^4$, where scars would show exceptionally large IPR as in Fig. 3(a). Because of the absence of degenerate level hybridization, the original scar components in Eq. (4) still dominate upon perturbation

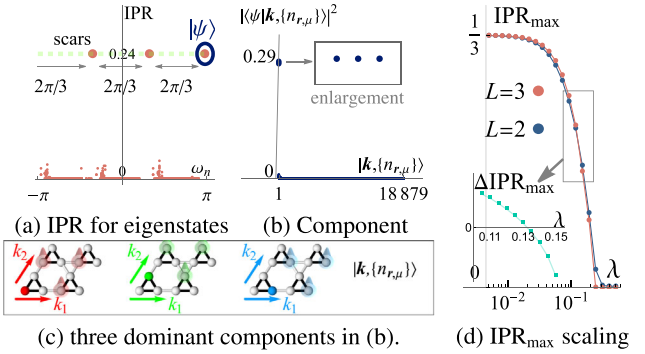

FIG. 3. Structure of Floquet eigenstates in $\boldsymbol{k} = \boldsymbol{0}$ sector. Other $\boldsymbol{k}$ sectors show essentially the same results. (a) Most eigenstates involve an extensive number of basis $|\boldsymbol{k}, \{n_{r\mu}\}\rangle$ leading to vanishing IPR, except for the three FBSs. (b) Expand for instance one FBS in the basis $|\boldsymbol{k}, \{n_{r\mu}\}\rangle$; we see it is dominated by three components depicted in (c), exactly as given by Eq. (4). (d) Scaling of the maximal IPR, where $\Delta\mathrm{IPR}_{\max} = \mathrm{IPR}^{(L=3)}_{\max} - \mathrm{IPR}^{(L=2)}_{\max}$ in the inset. Parameters are the same as in Fig. 1, and $L = 3$ for (a) and (b).

as in Figs. 3(b) and 3(c). The scaling of the largest IPRs in Fig. 3(d) reproduces the reference transition $\lambda_0 \approx 0.135$ as in Fig. 2(e).

Experimental relevance.—Small clusters studied above can be readily realized using the latest technology of quantum gas microscopes [62–64], which allows for manipulation and detection with single-site resolutions. We now further discuss cases with finite filling fractions relevant to wider ranges of experiments.

In principle, previous analytical results show that initial states populating more than one unit cell will chiefly overlap with nonscar ergodic eigenstates. Therefore, a finite filling fraction among all unit cells will eventually lead to a thermalizing behavior without dynamical signatures. However, there could exist a finite and predictable time window before decay to observe the scar DTCs due to scar localization.

To show it, we first take a closer look at Fig. 1(b). The initial state of putting N_b bosons on one site overlaps with all FBSs [perturbed Eq. (4)] in different $(\boldsymbol{k}, \ell)$ sectors; they interfere destructively everywhere except for the unit cell $\boldsymbol{r} = \boldsymbol{0}$, resulting in a real-space localization. As such, two scar DTCs localized in different regions will take time to sense the presence of and affect each other $\phi_2 n_{\mathrm{ol}}(n_{\mathrm{ol}} - 1)t_0 \sim 1$ by interactions, giving rise to the characteristic timescale t_0 to observe DTCs before decays. Here n_{ol} is the density overlap for two scar DTCs hypothetically left alone in a lattice. Then, one can predict that larger distance gives a smaller density overlap n_{ol}, which prolongs the scar DTC lifetime. Such expectations are verified numerically in the Supplemental Material [54] for two lattice settings relevant to the Berkeley platform. It confirms the possibility of observing DTC signatures with finite filling fractions over the experimentally accessible time, and further points out theoretically the controlling parameter for the DTC lifetime therein: the distance of initially populated cells.

Conclusion.—We show a distinct DTC phenomenon enforced by the analytically discovered FBSs. Its intrinsic Floquet and many-body nature stabilize spectral pairings against translation-invariant bilinear perturbations. Moreover, the new scheme of checking Floquet emergent degeneracy and scar spectral pairing indicates a possible procedure to unveil the long-sought universal mechanism behind clean DTCs in arbitrary dimensions. It is also tantalizing to incorporate more intricate crystalline spacegroup symmetries aside from translations into designing DTCs with unique structures and phenomena in clean systems.

This work is supported by the National Natural Science Foundation of China Grant No. 12174389 (B. H.), the NSF Grant No. PHY-1806362 (T. H. L., D. S.), the MURI-ARO Grant No. W911NF17-1-0323 through UC Santa Barbara (B. H., T. H. L., D. S., W. V. L.), AFOSR Grant No. FA9550-16-1-0006 (W. V. L.), and the Shanghai Municipal Science and Technology Major Project (Grant No. 2019SHZDZX01) (W. V. L.).

*phys.huang.biao@gmail.com
†wvliu@pitt.edu

[1] V. Khemani, A. Lazarides, R. Moessner, and S. L. Sondhi, Phase Structure of Driven Quantum Systems, Phys. Rev. Lett. **116**, 250401 (2016).
[2] D. V. Else, B. Bauer, and C. Nayak, Floquet Time Crystals, Phys. Rev. Lett. **117**, 090402 (2016).
[3] N. Y. Yao, A. C. Potter, I.-D. Potirniche, and A. Vishwanath, Discrete Time Crystals: Rigidity, Criticality, and Realizations, Phys. Rev. Lett. **118**, 030401 (2017).
[4] W. W. Ho, S. Choi, M. D. Lukin, and D. A. Abanin, Critical Time Crystals in Dipolar Systems, Phys. Rev. Lett. **119**, 010602 (2017).
[5] K. Sacha, Modeling spontaneous breaking of time-translation symmetry, Phys. Rev. A **91**, 033617 (2015).
[6] J. Zhang, P. W. Hess, A. Kyprianidis, P. Becker, A. Lee, J. Smith, G. Pagano, I.-D. Potirniche, A. C. Potter, A. Vishwanath, N. Y. Yao, and C. Monroe, Observation of a discrete time crystal, Nature (London) **543**, 217 (2017).
[7] S. Choi, J. Choi, R. Landig, G. Kucsko, H. Zhou, J. Isoya, F. Jelezko, S. Onoda, H. Sumiya, V. Khemani, C. von Keyserlingk, N. Y. Yao, E. Demler, and M. D. Lukin, Observation of discrete time-crystalline order in a disordered dipolar many-body system, Nature (London) **543**, 221 (2017).
[8] L. D. Landau and E. M. Lifshitz, *Statistical Physics*, Third Edition (Butterworth-Heinemann, Oxford, 1980).
[9] J. Rovny, R. L. Blum, and S. E. Barrett, Observation of Discrete-Time-Crystal Signatures in an Ordered Dipolar Many-Body System, Phys. Rev. Lett. **120**, 180603 (2018).
[10] S. Pal, N. Nishad, T. S. Mahesh, and G. J. Sreejith, Temporal Order in Periodically Driven Spins in Star-Shaped Clusters, Phys. Rev. Lett. **120**, 180602 (2018).
[11] X. Mi *et al.*, Time-crystalline eigenstate order on a quantum processor, Nature (London) **601**, 531 (2022).
[12] J. Randall, C. E. Bradley, F. V. van der Gronden, A. Galicia, M. H. Abobeih, M. Markham, D. J. Twitchen, F. Machado, N. Y. Yao, and T. H. Taminiau, Many-body–localized discrete time crystal with a programmable spin-based quantum simulator, Science **374**, 1474 (2021).
[13] A. Kyprianidis, F. Machado, W. Morong, P. Becker, K. S. Collins, D. V. Else, L. Feng, P. W. Hess, C. Nayak, G. Pagano, N. Y. Yao, and C. Monroe, Observation of a prethermal discrete time crystal, Science **372**, 1192 (2021).
[14] M. P. Estarellas, T. Osada, V. M. Bastidas, B. Renoust, K. Sanaka, W. J. Munro, and K. Nemoto, Simulating complex quantum networks with time crystals, Sci. Adv. **6**, eaay8892 (2020).
[15] P. Frey and S. Rachel, Realization of a discrete time crystal on 57 qubits of a quantum computer, Sci. Adv. **8**, eabm7652 (2022).
[16] C. W. von Keyserlingk, V. Khemani, and S. L. Sondhi, Absolute stability and spatiotemporal long-range order in floquet systems, Phys. Rev. B **94**, 085112 (2016).
[17] B. Huang, Y.-H. Wu, and W. V. Liu, Clean Floquet Time Crystals: Models and Realizations in Cold Atoms, Phys. Rev. Lett. **120**, 110603 (2018).
[18] A. Russomanno, F. Iemini, M. Dalmonte, and R. Fazio, Floquet time crystal in the Lipkin-Meshkov-Glick model, Phys. Rev. B **95**, 214307 (2017).

[19] T.-S. Zeng and D. N. Sheng, Prethermal time crystals in a one-dimensional periodically driven floquet system, Phys. Rev. B **96**, 094202 (2017).
[20] C. Lyu, S. Choudhury, C. Lv, Y. Yan, and Q. Zhou, Eternal discrete time crystal beating the heisenberg limit, Phys. Rev. Research **2**, 033070 (2020).
[21] W. C. Yu, J. Tangpanitanon, A. W. Glaetzle, D. Jaksch, and D. G. Angelakis, Discrete time crystal in globally driven interacting quantum systems without disorder, Phys. Rev. A **99**, 033618 (2019).
[22] K. Mizuta, K. Takasan, M. Nakagawa, and N. Kawakami, Spatial-Translation-Induced Discrete Time Crystals, Phys. Rev. Lett. **121**, 093001 (2018).
[23] R. E. Barfknecht, S. E. Rasmussen, A. Foerster, and N. T. Zinner, Realizing time crystals in discrete quantum few-body systems, Phys. Rev. B **99**, 144304 (2019).
[24] D. A. Abanin, E. Altman, I. Bloch, and M. Serbyn, Colloquium: Many-body localization, thermalization, and entanglement, Rev. Mod. Phys. **91**, 021001 (2019).
[25] D. V. Else, B. Bauer, and C. Nayak, Prethermal Phases of Matter Protected by Time-Translation Symmetry, Phys. Rev. X **7**, 011026 (2017).
[26] D. J. Luitz, R. Moessner, S. L. Sondhi, and V. Khemani, Prethermalization Without Temperature, Phys. Rev. X **10**, 021046 (2020).
[27] W. W. Ho and W. D. Roeck, A rigorous theory of prethermalization without temperature, arXiv:2011.14583.
[28] V. Khemani, R. Moessner, and S. L. Sondhi, A brief history of time crystals, arXiv:1910.10745.
[29] C. J. Turner, A. A. Michailidis, D. A. Abanin, M. Serbyn, and Z. Papić, Weak ergodicity breaking from quantum many-body scars, Nat. Phys. **14**, 745 (2018).
[30] A. Pizzi, D. Malz, G. De Tomasi, J. Knolle, and A. Nunnenkamp, Time crystallinity and finite-size effects in clean floquet systems, Phys. Rev. B **102**, 214207 (2020).
[31] H. Yarloo, A. Emami Kopaei, and A. Langari, Homogeneous floquet time crystal from weak ergodicity breaking, Phys. Rev. B **102**, 224309 (2020).
[32] T. H. Barter, T.-H. Leung, M. Okano, M. Block, N. Y. Yao, and D. M. Stamper-Kurn, Spatial coherence of a strongly interacting bose gas in the trimerized kagome lattice, Phys. Rev. A **101**, 011601(R) (2020).
[33] V. Khemani, C. R. Laumann, and A. Chandran, Signatures of integrability in the dynamics of rydberg-blockaded chains, Phys. Rev. B **99**, 161101(R) (2019).
[34] S. Choi, C. J. Turner, H. Pichler, W. W. Ho, A. A. Michailidis, Z. Papić, M. Serbyn, M. D. Lukin, and D. A. Abanin, Emergent SU(2) Dynamics and Perfect Quantum Many-Body Scars, Phys. Rev. Lett. **122**, 220603 (2019).
[35] H. Bernien, S. Schwartz, A. Keesling, H. Levine, A. Omran, H. Pichler, S. Choi, A. S. Zibrov, M. Endres, M. Greiner, V. Vuletić, and M. D. Lukin, Probing many-body dynamics on a 51-atom quantum simulator, Nature (London) **551**, 579 (2017).
[36] D. Bluvstein, A. Omran, H. Levine, A. Keesling, G. Semeghini, S. Ebadi, T. T. Wang, A. A. Michailidis, N. Maskara, W. W. Ho, S. Choi, M. Serbyn, M. Greiner, V. Vuletić, and M. D. Lukin, Controlling quantum many-body dynamics in driven rydberg atom arrays, Science **371**, 1355 (2021).
[37] N. Maskara, A. A. Michailidis, W. W. Ho, D. Bluvstein, S. Choi, M. D. Lukin, and M. Serbyn, Discrete Time-Crystalline Order Enabled by Quantum Many-Body Scars: Entanglement Steering via Periodic Driving, Phys. Rev. Lett. **127**, 090602 (2021).
[38] S. Sugiura, T. Kuwahara, and K. Saito, Many-body scar state intrinsic to periodically driven system, Phys. Rev. Research **3**, L012010 (2021).
[39] K. Mizuta, K. Takasan, and N. Kawakami, Exact floquet quantum many-body scars under rydberg blockade, Phys. Rev. Research **2**, 033284 (2020).
[40] H. Zhao, J. Vovrosh, F. Mintert, and J. Knolle, Quantum Many-Body Scars in Optical Lattices, Phys. Rev. Lett. **124**, 160604 (2020).
[41] B. Mukherjee, S. Nandy, A. Sen, D. Sen, and K. Sengupta, Collapse and revival of quantum many-body scars via floquet engineering, Phys. Rev. B **101**, 245107 (2020).
[42] J.-Y. Desaules, A. Hudomal, C. J. Turner, and Z. Papić, Proposal for Realizing Quantum Scars in the Tilted 1d Fermi-Hubbard model, Phys. Rev. Lett. **126**, 210601 (2021).
[43] S. Scherg, T. Kohlert, P. Sala, F. Pollmann, B. H. Madhusudhana, I. Bloch, and M. Aidelsburger, Observing non-ergodicity due to kinetic constraints in tilted Fermi-Hubbard chains, Nat. Commun. **12**, 4490 (2021).
[44] G.-X. Su, H. Sun, A. Hudomal, J.-Y. Desaules, Z.-Y. Zhou, B. Yang, J. C. Halimeh, Z.-S. Yuan, Z. Papić, and J.-W. Pan, Observation of unconventional many-body scarring in a quantum simulator, arXiv:2201.00821.
[45] A. Pizzi, J. Knolle, and A. Nunnenkamp, Period-*n* Discrete Time Crystals and Quasicrystals with Ultracold Bosons, Phys. Rev. Lett. **123**, 150601 (2019).
[46] A. Lazarides and R. Moessner, Fate of a discrete time crystal in an open system, Phys. Rev. B **95**, 195135 (2017).
[47] M. Serbyn, D. A. Abanin, and Z. Papić, Quantum many-body scars and weak breaking of ergodicity, Nat. Phys. **17**, 675 (2021).
[48] Y. Y. Atas, E. Bogomolny, O. Giraud, and G. Roux, Distribution of the Ratio of Consecutive Level Spacings in Random Matrix Ensembles, Phys. Rev. Lett. **110**, 084101 (2013).
[49] N. Regnault and R. Nandkishore, Floquet thermalization: Symmetries and random matrix ensembles, Phys. Rev. B **93**, 104203 (2016).
[50] L. D'Alessio, Y. Kafri, A. Polkovnikov, and M. Rigol, From quantum chaos and eigenstate thermalization to statistical mechanics and thermodynamics, Adv. Phys. **65**, 239 (2016).
[51] Due to limited sizes accessible here, we would postpone a more comprehensive examination of criticality to future work and only take λ_0 as a reference scar vanishing point.
[52] A. W. Sandvik, A. Avella, and F. Mancini, Computational studies of quantum spin systems, in *AIP Conference Proceedings* (AIP, 2010).
[53] In strongly disordered cases [1,2,16], spectral pairing happens for all eigenstates due to many-body localization. Here we use the terminology to describe similar behaviors for scars but due to different reasons.
[54] See Supplemental Materials at http://link.aps.org/supplemental/10.1103/PhysRevLett.129.133001 for details of Floquet perturbation treatment, entanglement entropy

calculations, and more experimental proposals. Additional Refs. [55–61] are included therein.

[55] C. K. Thomas, T. H. Barter, T.-H. Leung, M. Okano, G.-B. Jo, J. Guzman, I. Kimchi, A. Vishwanath, and D. M. Stamper-Kurn, Mean-Field Scaling of the Superfluid to Mott Insulator Transition in a 2d Optical Superlattice, Phys. Rev. Lett. **119**, 100402 (2017).

[56] T.-H. Leung, M. N. Schwarz, S.-W. Chang, C. D. Brown, G. Unnikrishnan, and D. Stamper-Kurn, Interaction-Enhanced Group Velocity of Bosons in the Flat Band of an Optical Kagome Lattice, Phys. Rev. Lett. **125**, 133001 (2020).

[57] C. D. Brown, S.-W. Chang, M. N. Schwarz, T.-H. Leung, V. Kozii, A. Avdoshkin, J. E. Moore, and D. Stamper-Kurn, Direct geometric probe of singularities in band structure, arXiv:2109.03354.

[58] G.-B. Jo, J. Guzman, C. K. Thomas, P. Hosur, A. Vishwanath, and D. M. Stamper-Kurn, Ultracold Atoms in a Tunable Optical Kagome Lattice, Phys. Rev. Lett. **108**, 045305 (2012).

[59] A. Quelle, C. Weitenberg, K. Sengstock, and C. M. Smith, Driving protocol for a floquet topological phase without static counterpart, New J. Phys. **19**, 113010 (2017).

[60] S. Taie, H. Ozawa, T. Ichinose, T. Nishio, S. Nakajima, and Y. Takahashi, Coherent driving and freezing of bosonic matter wave in an optical Lieb lattice, Sci. Adv. **1**, e1500854 (2015).

[61] A. Polkovnikov, Phase space representation of quantum dynamics, Ann. Phys. (N.Y.) **325**, 1790 (2010).

[62] M. Endres, H. Bernien, A. Keesling, H. Levine, E. R. Anschuetz, A. Krajenbrink, C. Senko, V. Vuletic, M. Greiner, and M. D. Lukin, Atom-by-atom assembly of defect-free one-dimensional cold atom arrays, Science **354**, 1024 (2016).

[63] M. E. Tai, A. Lukin, M. Rispoli, R. Schittko, T. Menke, D. Borgnia, P. M. Preiss, F. Grusdt, A. M. Kaufman, and M. Greiner, Microscopy of the interacting Harper–Hofstadter model in the two-body limit, Nature (London) **546**, 519 (2017).

[64] G. Semeghini, H. Levine, A. Keesling, S. Ebadi, T. T. Wang, D. Bluvstein, R. Verresen, H. Pichler, M. Kalinowski, R. Samajdar, A. Omran, S. Sachdev, A. Vishwanath, M. Greiner, V. Vuletić, and M. D. Lukin, Probing topological spin liquids on a programmable quantum simulator, Science **374**, 1242 (2021).